Chemical Physics 380 (2011) 1–8

Contents lists available at ScienceDirect

Chemical Physics

journal homepage: www.elsevier.com/locate/chemphys

Towards automated multi-dimensional quantum dynamical investigations of double-minimum potentials: Principles and example applications

Jan Sielk [a], H. Frank von Horsten [b], Bernd Hartke [a,*], Guntram Rauhut [c]

[a] Institut für Physikalische Chemie, Universität Kiel, Olshausenstr. 40, 24098 Kiel, Germany
[b] Department of Chemistry, PTCL, University of Oxford, South Parks Road, Oxford OX1 3QZ, United Kingdom
[c] Institut für Theoretische Chemie, Universität Stuttgart, Pfaffenwaldring 55, 70569 Stuttgart, Germany

ARTICLE INFO

Article history:
Available online 22 June 2010

Keywords:
Potential energy surface
Many-coordinate expansion
Ab-initio calculations
Quantum-mechanical wavepacket dynamics

ABSTRACT

A multi-coordinate expansion of potential energy surfaces has been used to perform quantum dynamical calculations for reactions showing double-minimum potentials. Starting from the transition state, a fully automated algorithm for exploring the multi-dimensional potential energy surface represented by arbitrary internal or normal coordinates allows for an accurate description of the relevant regions for vibrational dynamics calculations. An interface to our multi-purpose quantum-dynamics program MrPropa enables routine calculations for simple chemical reactions. Illustrative calculations involving potential energy surfaces obtained from explicitly-correlated coupled-cluster calculations, CCSD(T)-F12a, are provided for the tunneling splittings in the isotopologues of hydrogen peroxide and for reaction dynamics based on the enantiomeric inversion of PHDCl.

1. Introduction

While a multitude of program packages exists for all kinds of electronic structure calculations, the situation differs completely for quantum dynamical calculations: Each research group relies on its own program which usually is limited to certain purposes. Of course, there are a few exceptions, like the multi-configuration time-dependent Hartree (MCTDH) code [1] or the Car–Parinello program [2] and several others. Once higher accuracy is desired than offered by density functional theory (DFT), all quantum-dynamics programs rely on an interface to an electronic structure code or some intermediate program that assembles electronic single point calculations to a potential energy surface (PES) using some fitting or interpolation algorithms. This situation is very unfortunate as the calculation of some time-dependent properties is a major task for each individual system. In order to overcome this problem, the electronic structure code should be able to generate a fraction of the multi-dimensional potential energy surface relevant for the problem in an automated fashion, which subsequently can be read in by a multi-purpose quantum-dynamics code. Within the framework of vibrational self-consistent field theory (VSCF), several electronic structure codes allow for the automated calculation of the PES around a single (isolated) minimum [3,4]. Usually a many-mode expansion of the PES in terms of normal coordinates is used in order to provide a vibrationally relevant representation of the PES [5,6]. In order to represent the two minima of a double-minimum potential on equal footing, the expansion point should by placed in between the two structures. As a normal mode analysis is restricted to stationary points, the transition state representing the activation barrier is the most obvious choice. For example, quite recently, Bowman and co-workers [7–9] used an expansions of the PES in terms of normal coordinates starting from the transition state (or in terms of permutationally invariant redundant atomic pair distances, followed by a dynamics treatment in normal coordinates) to study the tunneling splittings in NH_3, H_3O^+ and other systems. Consequently, we have extended our fully automated surface generation code as implemented in the Molpro suite of *ab initio* programs [10] to the calculation of double-minimum potentials starting from the corresponding transition state. Moreover, rather than relying on normal coordinates only, any linear combination of normal coordinates, localized normal coordinates [11] or any internal coordinates can be used within the expansion of the PES. In all cases a many-coordinate representation of the potential, i.e.

$$V(q_1,q_2,\ldots,q_{3N-6}) = \sum_i V_i(q_i) + \sum_{i<j} V_{ij}(q_i,q_j) + \sum_{i<j<k} V_{ijk}(q_i,q_j,q_k) + \cdots, \quad (1)$$

has been used. Within VSCF calculations this expansion converges rather quickly and thus in most cases it can be truncated after

* Corresponding author. Tel.: +49 431 880 2753; fax: +49 431 880 1758.
E-mail address: hartke@phc.uni-kiel.de (B. Hartke).

0301-0104/$ - see front matter © 2010 Elsevier B.V. All rights reserved.
doi:10.1016/j.chemphys.2010.06.018

the 3rd order term. This, however, depends on the coordinates chosen and in certain cases, e.g. the vibrational spectrum of acetylene, high-order terms cannot be neglected [12]. However, the calculation of high-order terms does not necessarily constitute a computational bottleneck as efficient modeling schemes exist for an accurate estimation of such contributions [13,14]. Within an automatic PES generation the many-mode representation of the potential appears to be superior in comparison to other representations as it allows for the application of very efficient prescreening techniques and the simultaneous use of different electronic structure levels, which lead to significant speed-ups (see below). Once the PES, represented by a multitude of grid points, has been generated, it is transformed to a polynomial representation in order to avoid multi-dimensional integration steps. Dumped to disk, these polynomials constitute the interface to our multi-purpose quantum-dynamics package, MrPropa [15]. In this way, the study of dynamical properties is reduced to just one run of the electronic structure code, followed by various possible quantum-dynamics calculations.

As examples for our approach, we present model calculations based on PESs for the systems H_2O_2 and PHDCl. The first one of these systems, H_2O_2, has been studied extensively in previous work. Therefore, we also do not provide a comprehensive overview of the broad literature on this system but only quote a highly subjective, small selection here. Several potential energy surfaces have been generated, which have then been used to simulate many spectroscopic properties with various methods (see Refs. [16–18] and further references cited therein), particularly vibrational levels and tunneling splittings. Calculation of these quantities is a tedious task and requires highly accurate multi-dimensional calculations [7–9,18–22]. In contrast to the work of Quack and co-workers [18–20], who used a sophisticated analytical potential for H_2O_2, containing terms of different character and fitted to both experimental and *ab initio* information, in this work we use a purely *ab initio* approach. We would also like to emphasize that we do not intend to present yet another benchmark study on this same system. Instead, we demonstrate here that a general, automatic approach is capable of producing results of comparable quality. Similarly, our emphasis is on the seamless, semi-automatic interfacing of *ab initio* PES generation and dynamics, not on methodical advances in either of these parts alone, in contrast to other work on this system, e.g. by Luckhaus [21] who introduced new discrete variable representation approaches and contraction schemes.

For the second system, PHDCl, relatively little is known. Creve and Nguyen [23] have studied the influence of different substitution patterns on the inversion mechanism in phosphines, noting that the dominance of the "classical vertex inversion" is broken only upon introduction of more than one halogen atom. Dréan et al. [24] have investigated fluoro- and chlorophosphanes by millimeter-wave spectroscopy and high-level *ab initio* calculations. In both cases, only data for the pure isotopologues (PH_2X and PD_2X, X = F, Cl) are presented, not for the mixed species PHDCl under study here, but central characteristics like the inversion barrier height are in good agreement to our findings. We are not aware of further studies on the PHDCl system offering substantially deeper insights. Again, our intention is not to provide an in-depth study of this system; we do not even address PHDCl itself. Instead, as further explained in Section 6, we construct a model system based on the PHDCl PES and use it to demonstrate the versatility of our approach by calculating a different quantity, namely the cumulative reaction probability $N(E)$, based on the very same, automatic many-mode expansion.

In the following we will summarize key technical aspects of our fully automated surface generation code. After a brief listing of technical details, the seamless junction of this code with our general quantum dynamics package is highlighted by a presentation and discussion of the two application examples.

2. Automated calculation of multi-dimensional double-minimum potential energy surfaces

Our fully automated surface generation code for the calculation of double-minimum potentials makes use of several approximations and techniques for speeding up the calculations:

1. An iterative interpolation scheme, which systematically increases the number of coarse grid points, is used in order to limit the number of electronic structure calculations. This scheme, using one-dimensional polynomials, is based on a convergence criterion including the norm of the individual n-coordinate surfaces V_i, V_{ij}, etc. (cf. Eq. (1)). This results in different numbers of *ab initio* points but a balanced description of all the individual surfaces [3]. Moreover, it allows to control the quality of the PES by a single threshold.
2. A prescreening scheme can be used to avoid the calculation of negligible terms in the expansion of the potential, i.e. n-coordinate surfaces V_i, V_{ij}, etc. The criterion for skipping individual surfaces of nth order is based on the norm of the corresponding $(n-1)$th order surfaces. As a consequence the sums of the high-order terms in Eq. (1) are limited to significant contributions only, i.e. for some regions of the PES the expansion of the potential is truncated after the 2nd order terms while other regions still include 3rd or 4th order corrections.
3. Potential energy surfaces can be described by a multi-level scheme, i.e. terms of different order can be treated at different computational levels. In contrast to on-the-fly calculations this feature becomes only feasible once an expansion is used for the representation of the potential. Usually, the 1D terms are computed at the coupled-cluster level in combination with a large basis set, while 2D and 3D terms are treated at lower levels like MP2 or DFT [25]. Usually, multi-level schemes lead to speed-ups by one or two orders of magnitude.
4. High-order many-mode terms can be modeled [13] on the basis of the underlying 1D and 2D terms obtained from high-level electronic structure calculations. We use semiempirical MO theory as fit functions and reparametrize the intrinsic parameters by a least-squares criterion to the 1D and 2D terms. This allows for an efficient while still accurate calculation of 3D and 4D terms [13].
5. For the treatment of double-minimum potentials we found it important to be able to control the elongations along the individual coordinates separately. This allows for more control over the extension of the PES, in particular once a preference direction (along the imaginary mode) dominates the PES.
6. Based on global arrays, the program is parallelized in a way that the number of grid points to be computed are distributed among the nodes. Consequently, even massively parallel architectures with hundreds of processors can be used [26].
7. Although we allow for the use of different coordinates, i.e. normal coordinates, linearly combined normal coordinates, localized normal coordinates or internal coordinates, all calculations provided here refer to internal coordinates. The definition of the coordinates is given by the representation of the geometry of the molecule in the input stream of the electronic structure calculation.
8. Once the potential is expanded in rectilinear coordinates, symmetry can be exploited for all Abelian subgroups. This usually leads to a significant reduction of the number of coarse grid points and thus to considerable speed-ups. However, using internal coordinates neither symmetry nor dummy atoms can be used presently.

All these features allow for an efficient yet accurate determination of relevant parts of the PES. The program outlined above provides a representation of the PES in terms of grid points. However, a subsequent transformation of all the individual terms of the expansion to multi-dimensional polynomials was found to be more convenient for further use in our quantum-dynamics program [27].

3. Generation of potential energy surfaces

For testing the approach outlined above we have computed the tunneling splittings in the isotopologues of hydrogen-peroxide, i.e. H_2O_2, D_2O_2 and HOOD, and the enantiomeric inversion of PHDCl. Electronic structure calculations have been performed at the CCSD(T)-F12a/v*n*z-f12 level, where *n* denotes the cardinal number of the basis set. Explicitly correlated coupled-cluster calculations are much better suited for the generation of accurate potential energy surfaces than conventional CCSD(T) calculations, because much smaller orbital basis sets can be used. This reduces the I/O bottleneck in the corresponding Hartree–Fock calculations, which may be severe once thousands of *ab initio* calculations need to be performed. The MP2-F12 calculations, which are the first step in CCSD(T)-F12a calculations, were performed using the MP2-F12/3C(FIX) method described in detail in Refs. [28,29]. In this method the numerous two-electron integrals are computed using robust density fitting (DF) approximations [30,31] (DF was not used in the Hartree–Fock and CCSD(T)-F12 calculations). The aug-cc-pV*n*Z/MP2FIT basis sets of Weigend et al. [32] were used as auxiliary basis. For evaluating the Fock matrix (which is needed in the AO and RI basis sets) the v*n*z/OPTRI basis sets [33] were used. The v*n*z/OPTRI basis sets [33] were also used for the resolution of the identity (RI). The complementary auxiliary basis set (CABS) approach was employed, i.e., the union of the AO and RI basis sets was used to approximate the resolution of the identity. The perturbative CABS singles correction as described in Refs. [29,34] was applied in all F12 calculations. This significantly reduces the Hartree–Fock basis set error. Careful tests showed that the choice of the density fitting basis has only a negligible effect on the vibrational frequencies. The choice of the RI basis is more critical; however, we found that employing larger RI basis sets does not reduce the statistical errors. Tight CABS thresholds (10^{-9}) were used in order to minimize the number of functions that were deleted due to near linear dependencies. The number of functions was kept constant for all displacements. This guarantees smooth potential energy surfaces.

Within the automatic generation of the potential energy surface for the hydrogen peroxide isotopologues, 16 grid points along each internal coordinate (as shown in Fig. 1) were used to generate polynomials up to 6th order. The many-coordinate expansion of the potential (see Eq. (1)) has been truncated after the 3rd order terms; we have verified that the influence of the 4th order terms is negligible (see below). A multi-level approach has been used for an efficient calculation of the surface, i.e. the 1D and 2D terms were determined using triple-ζ basis sets, while the 3D and 4D terms were computed at the double-ζ level. This results in 1432 CCSD(T)-F12a/vtz-f12 and 6336 CCSD(T)-F12a/vdz-f12 single point calculations. Numerous applications using similar multi-level schemes have shown that such an approach is of sufficient accuracy for most purposes [25,35,36]. This holds true in particular for explicitly-correlated coupled-cluster theory, as CCSD(T)-F12a/vdz-f12 calculations are usually of higher accuracy than conventional CCSD(T)/cc-pVTZ calculations. Maximum elongations along the individual internal coordinates were determined iteratively, controlled by the maximum of the relative energy or the periodicity of the coordinates, e.g. in case of the torsion.

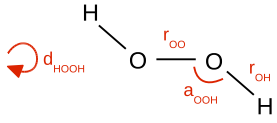

Fig. 1. The six internal coordinates of H_2O_2: *r* denotes distances, *a* angles and *d* is labeling the dihedral angle.

For PHDCl all electronic structure calculations have been performed using double-ζ rather than triple-ζ basis sets. The reason for this is the large number of *ab initio* calculations for a proper representation of the potential. The expansion of the potential has been truncated after the 3rd order terms. 24 grid points have been generated for each internal coordinate prior to the generation of the polynomial. This was found to be necessary due to the larger variations in the relative energy for PHDCl in comparison to hydrogen peroxide. Maximum elongations for the individual coordinates were determined iteratively as described above. The resulting points have been fitted to polynomials of order 8.

4. Kinetic energy operator

A crucial point in carrying out quantum dynamics for arbitrary *N*-atom systems is the complexity of the kinetic energy operator (KEO) when represented in curvilinear coordinates. In a general form the KEO may be written as

$$\widehat{T}(\mathbf{q},\partial_{\mathbf{q}}) = \sum_{i,j=1}^{3N-6} f_2^{ij}(\mathbf{q}) \frac{\partial^2}{\partial_{q_i}\partial_{q_j}} + \sum_{i=1}^{3N-6} f_1^{i}(\mathbf{q}) \frac{\partial}{\partial_{q_i}}, \tag{2}$$

where the "kinetic functions" f_2^{ij} and f_1^i can be expressed in terms of the (contravariant) metric tensor, the Jacobian determinant of the transformation from cartesian to curvilinear coordinates and their derivatives [37].

As in earlier work [38–40] we use the TNUM program [37,41] which is interfaced with our dynamics program in order to numerically evaluate the kinetic energy operator. Essentially, the only input necessary are the geometries of the molecule, **q**, which can conveniently be described by means of a *Z*-matrix as it is done for the potential part of the Hamiltonian. The kinetic functions f_2^{ij} and f_1^i are then calculated automatically on the required grid.

We note that first and second derivatives of the wavefunction appearing in Eq. (2) were calculated using the fast Fourier transform (FFT) technique [42,43]. This avoids the calculation of high-dimensional integrals since the derivatives can be directly multiplied by the f_2^{ij} and f_1^i functions on the given grid.

5. H_2O_2 and isotopologues: tunneling splittings

5.1. Computational details

Tunneling splittings of H_2O_2 have been calculated using the relaxation method introduced by Kosloff et al. [44]. Therein the time-dependent nuclear Schrödinger equation is propagated in imaginary time yielding the lowest eigenfunction of the system. Higher eigenfunctions can also be calculated by projecting out the lower ones during the propagation. For all calculations an energy threshold for the relaxation method of 10^{-8} kJ/mol was used.

Time propagation of the initial wavepacket was carried out using a Taylor expansion scheme developed by Lauvergnat et al. [45], which was originally designed for time-dependent Hamiltonians but is also applicable for time-independent Hamiltonians.

In all calculations 36 gridpoints were used for the FFT in the d_{HOOH} coordinate in the range from 5° to 355°. Twenty-one gridpoints in the range of 0.6–1.4 Å were used for the OH distance r_{OH}, 21 gridpoints in the range of 60–140° for the HOO angle a_{OOH}

and 29 gridpoints ranging from 1.1 to 1.8 Å for the OO distance r_{OO}. To ensure convergence of the relatively sparse grids, calculations with much denser grids were performed for some 1D, 2D and 3D cases. For higher-dimensional cases the denser grids were not computationally feasible anymore.

As it is well known, H_2O_2 has a tunneling splitting of its two lowest vibrational eigenfunctions caused by the double-minimum potential in the torsional coordinate. A simple one-dimensional cut through the PES does not yield the true tunneling splitting though, as other DOFs can couple to the torsion or simply change the potential barrier height due to geometry relaxation effects. In order to find out which of the other five internal DOFs contribute to the tunneling dynamics and which ones are just spectator modes, we systematically enlarge the dimensionality of the relaxation, starting from a simple rigid 1D cut along the torsional coordinate and ending up with a full six dimensional calculation, observing the effect on the tunneling splitting. Fig. 1 shows the six internal DOFs of H_2O_2. All "inactive" DOFs were fixed at their TS structure geometry for the PES evaluation as well as for the KEO.

5.2. Numerical results

Table 1 shows our results for the tunneling splitting in H_2O_2 and D_2O_2 calculated by the relaxation method. For both cases, full-dimensional 6D results are included (bottom row). It is not our intention to provide yet another benchmark study on this system but rather to demonstrate the flexibility of our automated approach. Also, substantial progress towards dynamics of higher-dimensional systems presently has to focus on using low-dimensional model approaches. Therefore, we take this opportunity to combine these two aspects here. Hence, Table 1 is devoted to an extensive comparison of the full 6D results to that of several lower-dimensional calculations, all of which could easily be performed with the automatic tandem setup described above. In each row of Table 1, checkmarks denote the active DOFs within this calculation, i.e. the corresponding cuts through the PES. All other (unchecked) DOFs were treated as spectator modes, as described above. Also shown is the resulting rigid potential energy barrier height of the double-minimum potential. This is to be compared to an energy difference of 4.444 kJ/mol (371.49 cm^{-1}) between the fully relaxed minimum and the first order saddle point.

Table 1
Tunneling splitting in cm^{-1} of the lowest-energy mode in H_2O_2 and its isotopologues; checkmarks denote DOFs which are treated explicitly in the wavepacket relaxation dynamics resulting in a nD FFT propagation.

r_{OH^1}	r_{OH^2}	r_{OO}	a_{OOH^1}	a_{OOH^2}	d_{HOOH}	HOOH	DOOD	Barrier
Exp.[a]						11.44	1.9	(kJ/mol)
1D:								
					✓	15.66	2.70	4.121
2D:								
			✓		✓	13.26	2.15	4.282
		✓			✓	15.62	2.67	4.126
✓					✓	13.99	2.44	4.062
3D:								
			✓	✓	✓	11.39	1.72	4.400
		✓	✓		✓	13.36	2.16	4.323
✓			✓		✓	11.62	1.91	4.284
✓		✓			✓	13.90	2.38	4.065
✓	✓				✓	12.50	2.21	4.130
4D:								
		✓	✓	✓	✓	11.43	1.69	4.541
✓			✓	✓	✓	9.85	1.47	4.404
✓	✓			✓	✓	10.25	1.67	4.291
✓	✓	✓			✓	12.38	2.13	4.069
✓		✓		✓	✓	11.72	1.92	4.327
5D:								
✓	✓		✓	✓	✓	8.52	1.26	4.409
6D:								
✓	✓	✓	✓	✓	✓	8.62	1.25	4.548

[a] Ref. [46,47,16].

Interpreting Table 1 from top to bottom, a rigid 1D cut through the PES along the torsional angle coordinate (d_{HOOH}) yields first results: 15.66 cm^{-1} (8.01 cm^{-1} for HOOD, 2.70 cm^{-1} for D_2O_2) for the tunneling splitting and 4.122 kJ/mol (344.57 cm^{-1}) for the barrier height. Of course, these are only very simple and rough first estimates. To enlarge the accuracy, other DOFs are successively added to the set of active coordinates and are treated explicitly during the wavepacket dynamics. From another point of view, one could also say that the dimensionality of the cuts through the global PES is further enlarged. Adding either one of the OH distances (r_{OH}) or one of the OOH angles (a_{OOH}) lowers the value of the tunneling splitting by 1.67 and 2.40 cm^{-1} respectively (0.26–0.55 cm^{-1} for D_2O_2), while addition of the OO distance (r_{OO}) leaves the value almost unchanged. The barrier height of the double well remains nearly unaffected (changes less than 0.1 kJ/mol $\approx$ 8 cm^{-1}), giving a first hint that coupling of the DOFs has a bigger impact on the tunneling splitting than on the barrier height.

This regularity is maintained upon further addition of DOFs to the set of active coordinates. Addition of the OO distance r_{OO} leaves the tunneling splitting almost unchanged, qualifying this coordinate as a spectator mode (as already noticed by Fehrensen et al. [19]). In contrast, adding r_{OH} or a_{OOH} reduces the value of the tunneling splitting by 1.5–2.0 cm^{-1} (0.2–0.5 cm^{-1} for D_2O_2). Thus we arrive at a 5D result of 8.52 cm^{-1} (HOOD: 4.10 cm^{-1}, D_2O_2: 1.26 cm^{-1}), where all internal coordinates except for the OO distance r_{OO} are treated explicitly. Because of our observation that addition of r_{OO} does not contribute to the tunneling splitting in all the diverse combinations of DOFs tested, we could "extrapolate" the full-dimensional 6D result, or rather: the 6D result should be identical with the 5D result to within ±0.1 cm^{-1}. The actual 6D result of 8.62 cm^{-1} (D_2O_2: 1.25 cm^{-1}) confirms this expectation. Also consistent with our earlier observation, the barrier height changes only slightly upon addition of active coordinates throughout all calculations. From this we tentatively conclude that the change in tunneling splitting is mainly caused by dynamic coupling of the DOFs rather than by their static influence on the barrier height. (It is conceivable but less likely that the barrier width changes while the barrier height remains the same.)

As obvious from the previous text and also from Table 1, the regularities observed above for H_2O_2 are valid also for D_2O_2 and HOOD. The reduction in the value of the change in tunneling splitting upon addition of r_{OD} and d_{OOD} is caused by the higher masses of the isotopes, which always reduce tunneling splittings. In a full 6D calculation for D_2O_2, our final result is 1.25 cm^{-1}, which again is in perfect agreement with the regularities deduced above.

The 4D–6D results in Table 1 have been produced with a PES expansion that was truncated after the 3-mode terms (cf. Eq. (1)). To check if the 4-mode terms have a noticeable impact on the tunneling splitting, all 4D and 5D calculations have been recalculated with the expansion truncated after the 4-mode terms (results not shown here). A detailed comparison of the results from corresponding 4D and 5D calculations without and with the 4-mode terms clearly demonstrates their negligible role. They have no influence on the barrier height at all, and only little impact on the tunneling splitting. The biggest change in tunneling splitting occurs for a set of four active coordinates, r_{OO}, both angles a_{OOH}, and d_{HOOH}, but even there the change only amounts to 0.4 cm^{-1}.

As a complementary view on the torsional motion in H_2O_2, we have additionally produced an effective 1D *ab initio* PES in d_{HOOH}, calculating 36 points at the CCSD(T)-F12a level (same basis set as quoted in Section 3), with all other DOFs fully relaxed at each

point. For this relaxed 1D PES, the barrier height is 4.444 kJ/mol (371.49 cm^{-1}), and we obtain a tunneling splitting of 12.8 cm^{-1}. The latter number is markedly smaller than the value of 15.66 cm^{-1} (cf. Table 1) for the 1D calculation in d_{HOOH} for a rigid-scan PES. In fact, this relaxed-1D splitting as well as our 4D splitting are closer to experiment than our 5D and 6D values. As we argue below, however, we view this agreement as fortuitous cancelation of small remaining errors.

Table 2 lists the lowest 6 excited vibrational states on this relaxed 1D PES, in direct comparison to the experimental values [16,46,47] and to the results of the (5 + 1) adiabatic approximation by Fehrensen et al. [19] (their (5 + 1) adiabatic approximation is similar but not identical to ours). Obviously, the results from this very simple relaxed 1D model agree quite well both with experiment and with the (5 + 1) adiabatic approximation by Fehrensen. The latter agreement is not very surprising, given the similar nature of the respective approximations. The good agreement with experiment indicates that this relaxed 1D model does capture some essential physics of the torsional motion (and tunneling), namely that the active coordinate d_{HOOH} moves significantly slower than the other five. This clearly is in line with our above interpretation, were strong couplings forced us to include almost all coordinates as active ones. On the other hand, this simple relaxed 1D PES diagnosis also clearly is of a less discriminatory nature: Above, we could diagnose one coordinate (r_{OO}) as inactive, which is in line with the findings by Fehrensen et al. [19]. This could not have been done on the basis of the 1D-relaxed PES alone.

As mentioned above, in Table 1 we would have obtained perfect agreement with experiment at the 3D or 4D level, where the obviously important coordinates (d_{HOOH} and the two a_{OOH}) are in the active set. Stepping up to 5D or 6D by adding both r_{OH} (and the indifferent r_{OO}) lowers the tunneling splitting by 3 cm^{-1} *away* from experiment. We would like to argue that this simply reveals the true result for the given PES, or equivalently, stepping back from 6D to 4D leads to an error of 3 cm^{-1} which fortuitously cancels (an)other error(s) of the same (small) magnitude.

One possible source for errors of this kind in the dynamics part is incomplete grid convergence in the high-D cases. As described in Section 5.1, however, we have tried to minimize these errors. Furthermore, following earlier treatments [18–20], we have restricted the dynamical treatment to $J = 0$. From classical analogies, errors induced by this approximation should be small, since the main effect of $J > 0$ should be on r_{OO} which was diagnosed above as a spectator mode. Actual $J > 0$ results [22] confirm this expectation. It appears more likely that residual errors are present in the electronic structure part. Recent results [12] indicate that frequencies calculated at the CCSD(T)-F12 level show mean errors of 4 cm^{-1} compared to experiment, which already is of the order of our present error. In fact, these 4 cm^{-1} already contain error compensation effects: Both core correlation and effects of higher excitations induce errors on the order of 10 cm^{-1} each. They partially cancel in standard frequency calculations (in a narrow region around a PES minimum), but this need not be the case when larger parts of a PES farther away from a minimum are of importance, as it is the case here.

Finally, we would like to emphasize again that the purpose of the present calculations on H_2O_2 and its isotopologues is not to produce a new, system-specific PES which then leads to perfect agreement with experimental data in dynamics calculations. Instead, we have demonstrated that a general approach with a fully automated PES generation and a standardized interface to a universal dynamics package yields results of a quality comparable to earlier studies dedicated to one particular system.

Table 2
Torsional spectrum H_2O_2 in cm^{-1}, relative to the fundamental.

Exp.[a]	(5 + 1)[b]	1D relaxed[c]
11.4	11.1	12.8
254.5	259.6	250.4
370.9	379.0	371.3
569.7	582.5	570.2
–	796.1	777.8
–	1028.6	1002.7

[a] Ref. [16,46,47].
[b] Ref. [19].
[c] This work.

6. PHDCl

6.1. Theoretical and computational details

In order to illustrate the generality of our automated methods further, in this section we calculate another important dynamical quantity, namely cumulative reaction probabilities (CRPs).

These CRPs are calculated by time-dependent wave packet propagation, employing the so-called transition-state wave packet (TSWP) approach by Zhang and Light [48]. For the sake of convenience we summarize the working equations of this method in an Appendix, as an aid for the interpretation of the results presented below. The full method is described nicely and in more detail elsewhere [49].

The dynamical system we employ for this purpose is a model system based upon the enantiomeric inversion of PHDCl (cf. Fig. 2). As mentioned in the Appendix, TSWPs are propagated starting from the transition state region. In order to avoid reflections of the TSWPs from the grid boundaries, absorbing (optical) potentials are located towards the "asymptotic regions". This is an intentional departure from the actual PHDCl enantiomeric inversion process depicted in Fig. 2. Due to the bound double well character of the PES, the true flux from reactants to products is canceled out by the flux of the reverse reaction. What we calculate here is a physically different setup. One could either imagine a strong interaction with the environment, making this barrier crossing motion incoherent and the CRP measurable. Alternatively, this setup could be interpreted as a generic model system for an incoherent reactive process, based on a realistic PES. In any case, we feel the calculation of the CRP in this model scenario is a better way to demonstrate the generality of our approach, rather than calculating energy levels and tunneling splittings as we already did in the H_2O_2 example.

The functional form of the optical potential employed goes back to works of Manolopoulos [50] and Zhang [51]. Here, we use the purely imaginary version which reads:

$$V_{\mathrm{opt}}(\mathbf{q}) = i\sum_{j=1}^{n} V_0 \exp\left(-\alpha \frac{q_j^{\max} - q_j}{q_j - q_j^{\star}}\right). \tag{3}$$

In Eq. (3), $q_j^{\max}$ denotes the end of the grid in the jth coordinate while $q_j^{\star}$ is the point where the optical potential becomes nonzero. Explicit values of these parameters, including the amplitude V_0 and the factor α appearing in the argument of the exponential function, are given in Table 3.

Table 4 summarizes the connectivity used and defines the names of the coordinates. The DOF describing the inversion is the dihedral angle ϕ, and the dividing surface between reactants and products is simply given by $s(\phi) = \phi - 180° = 0°$.

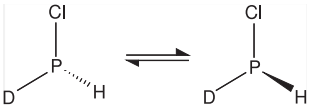

Fig. 2. Schematic illustration of the PHDCl inversion.

Table 3
Parameters of the absorbing potential. The top part of the table contains the values for $q_j^\star$ of Eq. (3), for the absorbing potentials on both sides of the transition state structure. Angles are given in degrees and distances in Å.

$\phi^\star$	140.0	220.0
rCl*	1.8	2.2
rH*, rD*	1.2	1.8
aH*, aD*	90.0	150.0

$V_0 = -800$ kJ/mol.
$\alpha = 1.0$.

Table 4
Z-matrix connectivities.

P						
Cl	1			rCl		
D	1	2		rD	aD	
H	1	2	3	rH	aH	ϕ

One-dimensional potential energy curves are shown in Fig. 3. In the relaxed case (red curve) all DOFs except for the dihedral angle are optimized at the CCSD(T)-F12a/vdz-f12 level on 36 points in the interval $\phi \in [5°, 355°]$. The classical barrier height for this reaction is $\Delta V_{\text{relax}} = 183.53$ kJ/mol. The green curve displays an 1D rigid cut of the full 6D PES, where the remaining DOFs are held fixed at the transition state geometry. Freezing the inactive coordinates, of course, changes the barrier height. It is, however, vital for the reduced dimensional CRP results presented later that the barrier height is made independent of the values at which the "spectator modes" are fixed. Hence, to achieve a meaningful comparison of differing numbers and selections of active DOFs, the rigid PESs are shifted by the energy difference between the relaxed and rigid barrier heights. Some examples of energy shifts $\Delta E_{\text{rigid}} = \Delta V_{\text{relax}} - \Delta V_{\text{rigid}}$ are given in Table 5.

Harmonic frequency calculations at the CCSD(T)-F12a/vdz-f12 level yield a zero-point energy corrected adiabatic barrier height of $\Delta V_{\text{adiab}} = 180.33$ kJ/mol, cf. Table 6. Additionally, anharmonic frequencies are calculated using the VCI technique. This results in a slightly increased barrier height of $\Delta V_{\text{adiab}}^{\text{VCI}} = 180.47$ kJ/mol.

Quantum dynamical calculations are performed using the TSWP method as outlined above for total angular momentum $J = 0$. We present a series of results with differing numbers n and selections of active DOFs up to $n = 3$. The number of grid points is taken to be

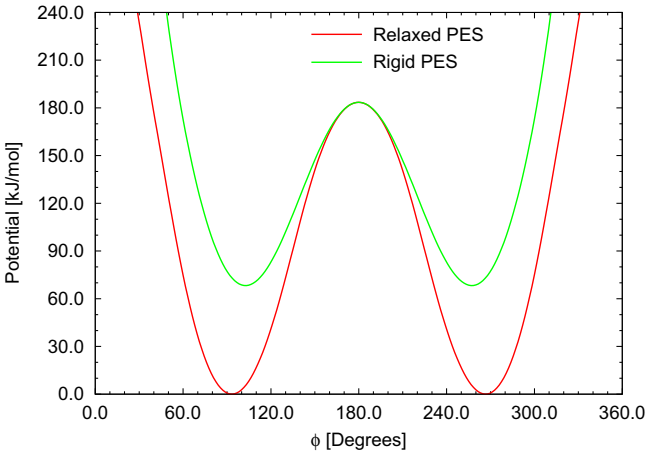

Fig. 3. One-dimensional relaxed (green) and rigid (red) potential energy curves as a functions of the inversion angle ϕ. In the rigid case, the inactive DOFs were fixed at the transition state values. (For interpretation of the references to colour in this figure legend, the reader is referred to the web version of this article.)

Table 5
Classical rigid barrier heights, ΔV_{rigid}, and energy shifts, ΔE_{rigid}, to compensate for the rigidity of the PESs. Quantities given in kJ/mol.

	ΔV_{rigid}	ΔE_{rigid}
1D ϕ (rigid)	115.26	68.27
2D ϕ + rH (D)	116.89	66.64
2D ϕ + aH (D)	150.31	33.22
2D ϕ + rCl	116.27	67.26
3D ϕ + rD + rH	118.80	64.73
3D ϕ + rH (D) + vH (D)	153.45	30.08

Table 6
Single-point energies, harmonic (ZPE) and anharmonic (VCI) zero-point energy corrections (CCSD(T)-F12/vdz-f12) at stationary points and the resulting classical and adiabatic reaction energies. All energies are given in kJ/mol.

	Energy	ZPE	VCI
Reactant	0.0	42.69	42.28
TS	183.53	39.49	39.22
ΔV_{adiab}	180.33		
$\Delta V_{\text{adiab}}^{\text{VCI}}$	180.47		

201 for the reaction coordinate ϕ while for the other active DOFs 50 points suffice for convergence. The time-dependent Schrödinger equation is solved using a symplectic integrators propagation scheme [52–54] of order 8. A time step of 0.01 fs is used for the first 10 fs where the correlation functions show a strongly oscillatory behavior. After that a value of 0.02 fs proves to be sufficient. The total propagation time varies between 120 and 150 fs from case to case. The matrix elements of the flux operator are calculated employing 180 particle-in-a-box basis functions in the ϕ coordinate. The nD product basis functions are constructed as the direct product of these 1D basis functions with the eigenfunctions of the $(n-1)$D Hamiltonian on the dividing surface, i.e. at a fixed ϕ value of 180°.

6.2. Reaction probabilities

The results of the CRP calculations for $n = 1, 2, 3$ are shown in Fig. 4. Additionally, the adiabatic vibrational barrier height $\Delta V_{\text{adiab}} = 180.33$ kJ/mol is included as vertical line to highlight quantum effects. All curves show a strictly monotonic increase in a TST-like fashion as function of total energy. Given the present double-minimum shape of the PES this is not surprising, or – in other words – an oscillatory behavior as it is reported for instance in heavy-light-heavy systems (see e.g. Refs. [55,56]) is not expected to be an issue here.

The most striking difference between the explicitly treated DOFs is the step width of the staircase structure. This can be explained quite easily by the quantization of states at the TS. Comparing for instance the 2D cases ϕ + rH (green) with ϕ + rD (blue), one sees that the step width is much smaller in the case where the distance to the deuterium atom is the second active coordinate. The reason for this, of course, is that due to the higher mass the energy levels are more closely spaced. As a result, the first vibrationally excited state turns on much "earlier" (i.e. at lower energies). In the extreme case where the distance to the chlorine atom is explicitly treated in the dynamics (orange curve), the staircase structure is nearly completely washed out. This is because the first excited state turns on at so much "earlier" energies that the ground state did not have "enough time" to reach its maximum value of unity before the next excited state is accessible. To quantify these arguments, we provide Table 7 with quantitative estimates for the expected widths of the staircase steps in the different reduced-dimensionality models.

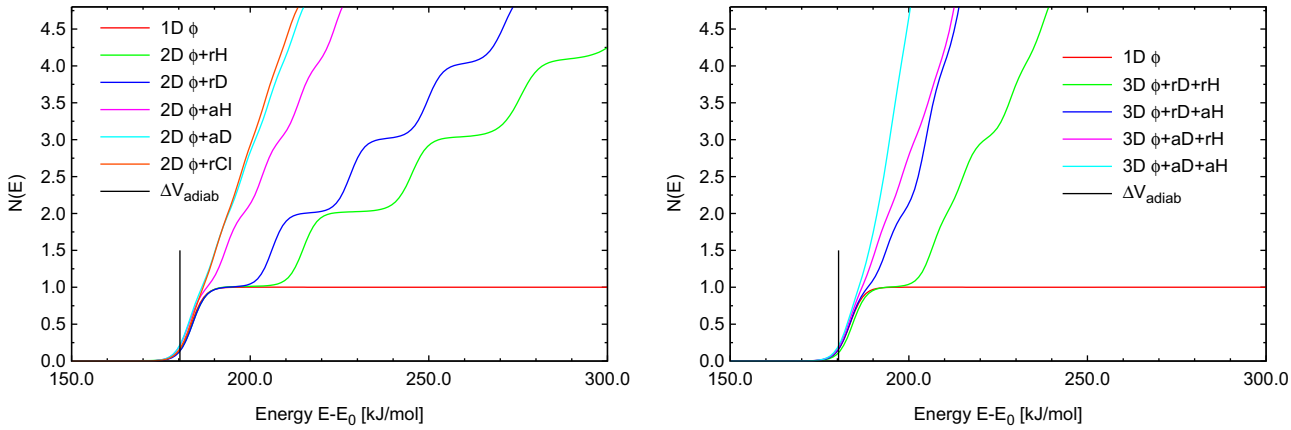

Fig. 4. Cumulative reaction probability $N(E)$ as function of the total energy above the PES minimum. Left panel: 1D and 2D results, right panel: 3D results. The energy shift is given by $E_0 = \mathrm{ZPE}^{\ddagger} - \Delta E_{\mathrm{rigid}}$. Note that the 1D result was obtained by employing a PES fully relaxed in all other DOFs, i.e. the green curve in Fig. 3. (For interpretation of the references to colour in this figure legend, the reader is referred to the web version of this article.)

This line of argumentation carries over analogously to the presented 3D results. With increasing number of active coordinates the density of states increases much more rapidly as a function of energy. Therefore (after the first step) all 3D curves have a much smoother shape compared to the 2D calculations. One might notice that in the lower energy regions some of the 3D curves are not quite on top of the result of the fully relaxed 1D PES. This is most apparent for the ϕ + rD + rH case (green), where the curve is slightly shifted to higher energies. Therefore, freezing the inactive DOFs in this case appears to be not a good approximation because it shifts the reaction onset away from is "true value" which would be obtained by using a relaxed potential energy surface.

In conclusion, the presented 2D and 3D results evidently already capture the most important dynamical aspects of this reaction. Or, in other words, the results have converged with respect to the number of active DOFs. Hence, we refrain from performing higher-dimensional calculations. These would computationally be very demanding since quite a few (4D or even higher dimensional) TSWPs would have to be propagated. On the other hand, our results clearly demonstrate that reduced dimensional calculations can yield very reliable results. This might not be of crucial importance for the systems under study here, but is the key to study other polyatomics with more than say five atoms. In cases like these, the curse of dimensionality forbids any *general* but yet *exact* quantum-dynamical treatment, and reduced-dimensional approaches form an elegant way to tackle these kinds of problems. Nonetheless, even if in the present case freezing the inactive DOFs often turns out to be a rather good approximation, it is clearly desirable to employ a relaxed PES. Work into that direction is currently in progress.

Table 7
ZPE corrections at the transition state (in kJ/mol) obtained by diagonalization of the $(n-1)$D Hamiltonian. $\Delta E^{\ddagger}_{\mathrm{vib}}$ is the energy difference between the ground and first vibrationally excited state which gives an estimate of the (first) step width of the $N(E)$ curves.

	$\mathrm{ZPE}^{\ddagger}$	$\Delta E^{\ddagger}_{\mathrm{vib}}$
2D ϕ + *r*H	15.35	30.71
2D ϕ + *r*D	10.91	22.21
2D ϕ + *a*H	5.70	10.24
2D ϕ + *a*D	4.39	7.46
2D ϕ + *r*Cl	3.52	6.93
3D ϕ + *r*D + rH	26.24	22.18
3D ϕ + *r*D + *a*H	16.37	10.22
3D ϕ + *a*D + *r*H	19.71	7.44
3D ϕ + *a*D + *a*H	9.99	6.37

7. Summary and conclusions

The investigation of reactions beyond a one-dimensional approximation usually is a tedious and time-consuming task. While molecular properties derived from a one-dimensional intrinsic reaction coordinate (IRC) are often of reasonable quality, for many applications multi-dimensional effects need to be considered explicitly. Of course, in principle one could adapt each investigation to the specific topology of the molecular system under study and thus obtain fairly accurate results. An example for this is the complicated setup of system-tailored kinetic energy operators. In practice, a fully automated – yet reliable – standard procedure for studying such reactions is still missing. In this study we have presented a scheme which we would consider semi-automated. While the generation of the multi-dimensional potential energy surface is fully automated, the subsequent quantum dynamical studies require several test calculations in order to determine converged results with respect to the number and selection of important coordinates. However, efforts are made to overcome these limitations.

Employing a many-mode expansion around the transition state allows to introduce a variety of methods (detailed in Section 2) to reduce the computational effort of PES generation in a systematic and well-controlled manner. As illustrated in our first application example, this makes it possible to generate a highly accurate PES with high-level *ab initio* methods without having to calculate PES points in full dimensionality. This accurate but economic PES generation is complemented by a universal reaction dynamics approach that enables us to employ various reduced-dimensionality models and thus to identify reaction-promoting modes and spectator modes. An analysis of the minimum energy path with respect to the contributing internal coordinates within the many-mode expansion of the potential should in principle allow for an automated selection of the most relevant coordinates for the quantum-dynamical calculations.

In future work, we intend to investigate other reactive systems, including higher-dimensional ones. In particular, an investigation of so-called plateau reactions, which are described by a plateau of almost constant energy in the region of the (formal) transition state should profit from the approach outlined above, because the one-dimensional intrinsic reaction coordinate is hardly able

to describe such reactions [57–59]. To this end, we plan to incorporate the adaptive propagation scheme introduced by some of the present authors [40,60]. This scheme avoids rectangular direct-product grids and thus also helps to avoid outer regions in the many-mode expansion terms where polynomial fits tend to degrade.

Acknowledgments

It is a pleasure to thank Sarah Remmert and Ivan Ljubić for many useful discussions. Financial support by the German Science Foundation (DFG) through grants Ha 2498/6-1 and Ra 656/9-1 is gratefully acknowledged.

Appendix

In order to avoid the cumbersome calculation of state-to-state properties, the trace expression by Miller et al. [61] is employed:

$$N(E) = \frac{(2\pi\hbar)^2}{2}\mathrm{tr}\left[\delta\left(E-\widehat{H}\right)\widehat{F}\delta\left(E-\widehat{H}\right)\widehat{F}\right]. \tag{4}$$

The trace in Eq. 4 can be evaluated in different ways; for clarity we briefly list the recipe used here:

1. Define a dividing surface $s(\mathbf{q}) = 0$ separating reactants from products.
2. Calculate a matrix representation of the flux operator:

$$\widehat{F} = \frac{i}{\hbar}\left[\widehat{H}, \Theta(s(\mathbf{q}))\right], \tag{5}$$

   where Θ is the Heaviside step function which is defined to be smaller than zero on the reactant side and larger than zero on the product side. The explicit expression of the matrix elements for a general kinetic energy operator can be found in Ref. [62].
3. By diagonalization of the flux operator matrix one obtains eigenvalues $\pm\lambda_{k\in\mathbb{K}}$ and eigenfunctions $\langle\mathbf{q}|\pm k \in \mathbb{K}\rangle$ (TSWPs). In the one-dimensional case, the set $\mathbb{K}$ contains only unity as element since a 1D flux operator has only two non-zero eigenvalues of opposite signs [63]. In the multi-dimensional case the set is given by $\mathbb{K} = \{1,\ldots,K\}$, where K is the number of (product) basis functions in the DOF(s) other than the reaction coordinate.
4. The TSWPs are propagated forward and backward in time which results in correlation functions:

$$C_{\pm k,\pm k'}(t) = \left\langle \pm k\left|\mathrm{e}^{-i\widehat{H}t/\hbar}\right|\pm k'\right\rangle. \tag{6}$$

5. Fourier transform the correlation functions, i.e.

$$\left\langle \pm k\left|\delta(E-\widehat{H})\right|\pm k'\right\rangle = \frac{1}{2\pi\hbar}\int_{-\infty}^{\infty}\mathrm{e}^{iEt/\hbar}C_{\pm k,\pm k'}(t)dt. \tag{7}$$

6. Summation over the Fourier transformed correlation functions yields the cumulative reaction probability (CRP):

$$N(E) = (2\pi\hbar)^2\sum_{k,k'=1}^{K}\lambda_k\lambda_{k'}\left\{\left|\left\langle +k\left|\delta(E-\widehat{H})\right|+k'\right\rangle\right|^2 - \left|\left\langle -k\left|\delta(E-\widehat{H})\right|+k'\right\rangle\right|^2\right\}. \tag{8}$$

References

[1] U. Manthe, H.D. Meyer, L.S. Cederbaum, J. Chem. Phys. 97 (1992) 3199.
[2] M. Parrinello, W. Andreoni, CPMD Consortium. <http://www.cpmd.org/>.
[3] G. Rauhut, J. Chem. Phys. 121 (2004) 9313.
[4] D. Toffoli, J. Kongsted, O. Christiansen, J. Chem. Phys. 127 (2007) 204106.
[5] S. Carter, S.J. Culik, J.M. Bowman, J. Chem. Phys. 107 (1997) 10459.
[6] S. Carter, J.M. Bowman, L.B. Harding, Spectrochim. Acta A 53 (1997) 1179.
[7] E. Kamarchik, Y. Wang, J. Bowman, J. Phys. Chem. A 113 (2009) 7556.
[8] Y. Wang, J.M. Bowman, J. Chem. Phys. 129 (2008) 121103.
[9] Y. Wang, B.J. Braams, J.M. Bowman, S. Carter, D.P. Tew, J. Chem. Phys. 128 (2008) 224314.
[10] H.-J. Werner, P.J. Knowles, R. Lindh, F.R. Manby, M. Schütz, et al., Molpro, Development Version 2008.3, A Package of Ab initio Programs. <http://www.molpro.net>, 2008.
[11] G. Rauhut, J. Chem. Phys. 127 (2007) 184109.
[12] G. Rauhut, G. Knizia, H.-J. Werner, J. Chem. Phys. 130 (2009) 54105.
[13] G. Rauhut, B. Hartke, J. Chem. Phys. 131 (2009) 14108.
[14] E. Matito, D. Toffoli, O. Christiansen, J. Chem. Phys. 130 (2009) 134104.
[15] H.F. von Horsten, J. Sielk, B. Hartke, MrPropa, A Program Suite for Quantum-Mechanical Reaction Dynamics. <http://www.mrpropa.de>.
[16] L.B. Harding, J. Phys. Chem. 93 (1989) 8004.
[17] A. Willets, J.F. Gaw, N.C. Handy, S. Carter, J. Mol. Spectrosc. 135 (1989) 370.
[18] B. Kuhn, T.R. Rizzo, D. Luckhaus, M. Quack, M.A. Suhm, J. Chem. Phys. 111 (1999) 2565.
[19] B. Fehrensen, D. Luckhaus, M. Quack, Chem. Phys. 338 (2007) 90.
[20] B. Fehrensen, D. Luckhaus, M. Quack, Chem. Phys. Lett. 300 (1999) 312.
[21] D. Luckhaus, J. Chem. Phys. 113 (2000) 1329.
[22] S.Y. Lin, H. Guo, J. Chem. Phys. 119 (2003) 5867.
[23] S. Creve, M.T. Nguyen, J. Phys. Chem. A 102 (1998) 6549.
[24] P. Dréan, M. Paplewski, J. Demaison, J. Breidung, W. Thiel, H. Beckers, H. Bürger, Inorg. Chem. 35 (1996) 7671.
[25] K. Pflüger, M. Paulus, S. Jagiella, T. Burkert, G. Rauhut, Theor. Chem. Acc. 114 (2005) 327.
[26] T. Hrenar, H. Werner, G. Rauhut, J. Chem. Phys. 126 (2007) 134108.
[27] M. Neff, G. Rauhut, J. Chem. Phys. 131 (2009) 124129.
[28] H.-J. Werner, T.B. Adler, F.R. Manby, J. Chem. Phys. 126 (2007) 164102.
[29] G. Knizia, H.-J. Werner, J. Chem. Phys. 128 (2008) 154103.
[30] F.R. Manby, J. Chem. Phys. 119 (2003) 4607.
[31] A.J. May, F.R. Manby, J. Chem. Phys. 121 (2004) 4479.
[32] F. Weigend, A. Köhn, C. Hättig, J. Chem. Phys. 116 (2002) 3175.
[33] K.E. Yousaf, K.A. Peterson, J. Chem. Phys. 129 (2008) 184108.
[34] T.B. Adler, G. Knizia, H.-J. Werner, J. Chem. Phys. 127 (2007) 221106.
[35] G. Rauhut, T. Hrenar, Chem. Phys. 346 (2008) 160.
[36] K. Yagi, S. Hirata, K. Hirao, Theor. Chem. Acc. 127 (2007) 34111.
[37] D. Lauvergnat, A. Nauts, J. Chem. Phys. 116 (2002) 8560.
[38] H.F. von Horsten, G. Rauhut, B. Hartke, J. Phys. Chem. A 110 (2006) 13014.
[39] H.F. von Horsten, B. Hartke, Chem. Phys. 338 (2007) 160.
[40] J. Sielk, H.F. von Horsten, F. Krüger, R. Schneider, B. Hartke, Phys. Chem. Chem. Phys. 11 (2009) 463.
[41] D. Lauvergnat, E. Baloïtcha, G. Dive, M. Desouter-Lecomte, Chem. Phys. 306 (2006) 500.
[42] R. Kosloff, The Fourier method, in: Numerical Grid Methods and Their Applications to Schrödinger Equation, NATO ASI Series C, vol. 412, Springer, Dordrecht, 1993, p. 175.
[43] D. Kosloff, R. Kosloff, J. Comput. Phys. 52 (1983) 35.
[44] R. Kosloff, H. Tal-Ezer, Chem. Phys. Lett. 127 (1986) 223.
[45] D. Lauvergnat, S. Blasco, X. Chapuisat, A. Nauts, J. Chem. Phys. 126 (2007) 204103.
[46] R.H. Hunt, R.A. Leacock, J. Chem. Phys. 45 (1966) 3141.
[47] P. Helminger, W.C. Bowman, F.C.D. Lucia, J. Mol. Spectrosc. 85 (1981) 120.
[48] D.H. Zhang, J.C. Light, J. Chem. Phys. 104 (1996) 6184.
[49] B. Lasorne, F. Gatti, E. Baloïtcha, H.-D. Meyer, M. Desouter-Lecomte, J. Chem. Phys. 121 (2004) 644.
[50] D.E. Manolopoulos, Talk at the "Charles Coulson Summer School in Theoretical Chemistry", University of Oxford, Oxford, 1996.
[51] J.-Y. Ge, J.Z.H. Zhang, J. Chem. Phys. 108 (1998) 1429.
[52] S.K. Gray, J.M. Verosky, J. Chem. Phys. 100 (1994) 5011.
[53] S.K. Gray, D.E. Manolopoulos, J. Chem. Phys. 104 (1996) 7099.
[54] D.E. Manolopoulos, S.K. Gray, J. Chem. Phys. 102 (1995) 9214.
[55] S.T. Banks, D.C. Clary, Phys. Chem. Chem. Phys. 9 (2007) 933.
[56] S.M. Remmert, S.T. Banks, D.C. Clary, J. Phys. Chem. A 113 (2009) 4255.
[57] S. Schweiger, G. Rauhut, J. Phys. Chem. A 110 (2006) 2816.
[58] S. Schweiger, B. Hartke, G. Rauhut, Phys. Chem. Chem. Phys. 7 (2005) 493.
[59] S. Schweiger, B. Hartke, G. Rauhut, Phys. Chem. Chem. Phys. 6 (2004) 3341.
[60] B. Hartke, Phys. Chem. Chem. Phys. 8 (2006) 3627.
[61] W.H. Miller, S.D. Schwartz, J.W. Tromp, J. Chem. Phys. 79 (1983) 4889.
[62] E. Baloïtcha, B. Lasorne, D. Lauvergnat, G. Dive, Y. Justum, M. Desouter-Lecomte, J. Chem. Phys. 117 (2002) 727.
[63] T.J. Park, J.C. Light, J. Chem. Phys. 88 (1988) 4897.